

Imaging Plates for Use with Synchrotron Radiation

Yoshiyuki Amemiya

Photon Factory, National Laboratory for High Energy Physics, Oho 1-1 Tsukuba, Ibaraki 305, Japan

(Received 27 May 1994; accepted 27 June 1994)

This review summarizes the principles and performance characteristics of the imaging-plate (IP) X-ray area detector, which is based on the photo-stimulable phosphor $\text{BaF}(\text{Br},\text{I}):\text{Eu}^{2+}$, together with some of its applications at the Photon Factory. The photo-stimulable phosphor can temporarily store an X-ray image. The stored image is read out by measuring the intensity of luminescence, which is stimulated by an He–Ne laser beam scanning the phosphor surface. The IP has a spatial resolution of $170\ \mu\text{m}$ (FWHM) with a pixel size of $100 \times 100\ \mu\text{m}$ and area sizes ranging from 127×127 to $201 \times 400\ \text{mm}^2$. The dynamic range is over $1:10^5$. The detective quantum efficiency, which is a function of exposure level, is more than 80% for 8–20 keV X-rays at medium exposure levels. The background noise level is equivalent to less than 3 X-ray photons/pixel of 8 keV. The precision in intensity measurement is 0.5–1% at best. These performance characteristics of the IP depend largely on the performance of the IP readout system. Two applications of the IP to time-resolved measurements are discussed: one is based on a cinema method which achieves a 0.3 s time resolution for 40 exposures of size $127 \times 127\ \text{mm}^2$, and the other uses the IP as a linear detector of length 200 mm with a $23\ \mu\text{s}$ time resolution for a time period of 46 ms, based on the streak-camera method.

Keywords: imaging plates; X-ray detectors; X-ray diffraction.

1. Introduction

The requirements for X-ray detectors, which play an important role in X-ray diffraction experiments, are more strict when they are used in combination with synchrotron radiation as an intense X-ray source. Among the various requirements for X-ray area detectors, some of the most fundamental are: (i) a high detective quantum efficiency (DQE), (ii) a wide dynamic range, (iii) a linearity of response, (iv) a high spatial resolution, (v) a large active-area size, (vi) a uniformity of response and (vii) a high count-rate capability. The last requirement is most crucial in experiments using synchrotron radiation in order to make the best use of the high X-ray flux.

It has been shown experimentally that the performance characteristics of the imaging plate (IP) meet the above fundamental requirements for X-ray detectors for experiments with synchrotron radiation (Miyahara, Takahashi, Amemiya, Kamiya & Satow, 1986). The usefulness of the IP has also been demonstrated by X-ray diffraction experiments with contracting muscle (Amemiya, Wakabayashi, Tanaka, Ueno & Miyahara, 1987): the high DQE, wide dynamic range and unlimited instantaneous count-rate capability of the IP resulted in a sufficient reduction of the exposure time and hence made it possible to record a clear X-ray diffraction pattern, with up to 2 nm axial spacing, from a contracting frog skeletal muscle in as little as 10 s with synchrotron radiation.

The IP has also enabled protein crystallographers to obtain more accurate data sets with a reduced X-ray dosage and a shortened exposure time on protein crystals. This

reduction minimizes the radiation damage to the crystals and their instability during X-ray exposure. In practice, a full data set could be obtained from one crystal with a Weissenberg or an oscillation camera before the crystal was damaged by radiation, and with a better signal-to-noise ratio than with film (Miyahara, Takahashi, Amemiya, Kamiya & Satow, 1986; Sakabe, 1987). Thus, the IP has been used both intensively and extensively in experiments using synchrotron radiation during recent years.

In this review article, the principles and performance of the IP are summarized in §§2 and 3, respectively. In §4, an IP readout system which has been developed at the Photon Factory is described as an example. In §5, the apparatus and applications to time-resolved measurements with the IP are described.

2. Principles

The IP is a flexible plastic plate which is coated with bunches of very small crystals (grain size: about $5\ \mu\text{m}$) of photo-stimulable phosphor (previously $\text{BaFBr}:\text{Eu}^{2+}$, recently $\text{BaF}(\text{Br},\text{I}):\text{Eu}^{2+}$) by using an organic binder. The composite structure of the IP is shown in Fig. 1. The photo-stimulable phosphor is capable of storing a fraction of the absorbed X-ray energy. When later stimulated by visible light, it emits photo-stimulated luminescence (PSL), the intensity of which is proportional to the absorbed X-ray intensity (Sonoda, Takano, Miyahara & Kato, 1983).

The mechanism of the PSL is illustrated in Fig. 2; when the IP absorbs incoming X-rays, some of the electrons in

the valence band are pumped up to the conduction band of the phosphor crystals. (This corresponds to ionization of Eu^{2+} to Eu^{3+} .) The electrons, in turn, are trapped in Br^- and F^- vacancies, which were intentionally introduced into the phosphor crystals during the manufacturing process, forming temporary color centers, termed *F* centers. Exposure to visible light again pumps up the trapped electrons so that they generate energy for luminescence, while returning to the valence band of the crystal. (This process corresponds to a recombination of electrons with Eu^{3+} ions, resulting in Eu^{2+} luminescence.) Because the response time of the PSL is as short as $0.8 \mu\text{s}$, it is possible to read an X-ray image with a speed of $5\text{--}10 \mu\text{s}$ per pixel with high efficiency. The PSL is based on the allowable transition from $5d$ to $4f$ of Eu^{2+} . The wavelength of the PSL ($\lambda \approx 390 \text{ nm}$) is reasonably separated from that of the stimulating light ($\lambda = 632.8 \text{ nm}$), allowing it to be collected by a conventional high-quantum-efficiency photo-multiplier tube (PMT). The output of the PMT is amplified and converted to a digital image, which can be processed by a computer. The residual image on the IP can be completely erased by irradiation with visible light, to allow repeated use. The IP is easy to handle, because it is flexible, like a film, and can be kept under light before exposure to X-rays.

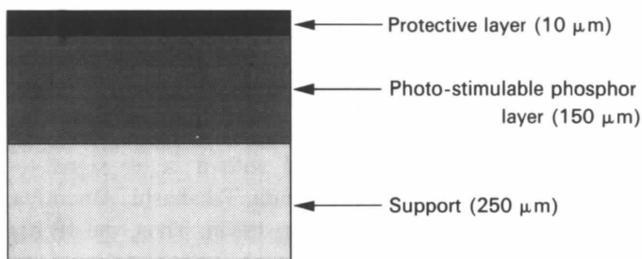


Figure 1
Composite structure of the imaging plate.

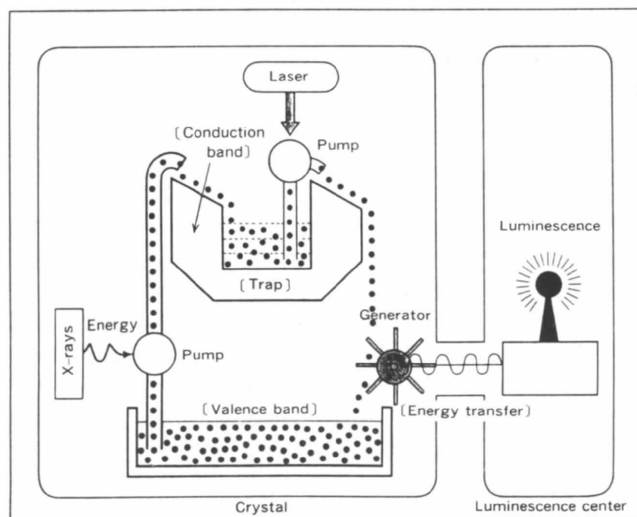


Figure 2
Mechanism of photo-stimulated luminescence (Miyahara, 1989).

3. Performance

The IP has excellent performance characteristics as an X-ray area detector. The principal characteristics are summarized below.

3.1. Detective quantum efficiency

The detective quantum efficiency (DQE) is defined as

$$\text{DQE} = (S_o/N_o)^2 / (S_i/N_i)^2$$

where S = signal and N = noise (standard deviation of signal) and subscripts o and i refer to the output and input, respectively. The measured DQE of the IP is shown as a function of the X-ray exposure level in Fig. 3. For comparison, the measured DQE of a high-sensitivity X-ray film (Kodak DEF-5) is also shown. The higher DQE of the IP compared with X-ray film is attributed partially to the higher absorption efficiency of the IP phosphor for X-rays. The advantage of the IP over X-ray film in DQE is clearly enhanced at lower exposure levels. This arises from the fact that the background noise level of the IP is much smaller than that of X-ray film. The background noise level of the IP usually corresponds to a signal level of less than 3 X-ray photons/ $(100 \mu\text{m})^2$. This value compares favorably with the chemical 'fog' level of X-ray film, which amounts to 1000 X-ray photons per equivalent area. It should be noted that the background noise level of the IP depends largely on the performance of the IP readout system. The level is as small as that of a single X-ray photon with the drum-type IP readout system described in §4. From Fig. 3, one can see that the DQE of the IP becomes lower at higher exposure levels, and that there is no significant difference in the DQE between the IP and X-ray film at highest exposure level. This is attributed to the fact that the relative uncertainty of the signal of the IP is saturated to $\sim 1\%$. Fig. 4 shows the relative uncertainty of the signal of the IP and X-ray film as a function of the X-ray exposure level. It is shown

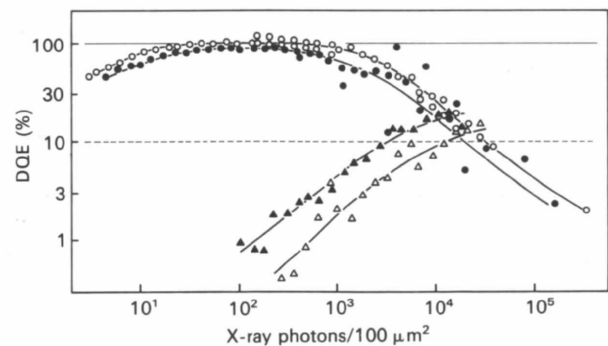


Figure 3
Measured detective quantum efficiency of the imaging plate and high-sensitivity X-ray film as a function of the exposure level. The circles correspond to the imaging plate (with the FCR 101 readout system, Fuji Film Co. Ltd), triangles to the X-ray film (Kodak DEF-5). The filled symbols are with 8.9 keV radiation, and open symbols with 19.6 keV radiation. The solid line indicates a noiseless counter of 100% absorption efficiency (ideal detector). The dashed line indicates a noiseless counter of 10% absorption efficiency (Amemiya & Miyahara, 1988).

that the relative uncertainties of both the IP and X-ray film deviate from an ideal detector at higher exposure levels. The saturation of the relative uncertainty of the IP results from 'system fluctuation noise'. Fig. 5 shows the propagation of signal and noise as well as the introduction of noise in the system. The origins of the system fluctuation noise are non-uniformity of absorption, non-uniformity of the color-center density, fluctuation of the laser intensity, non-uniformity of PSL collection, and fluctuation of the high-voltage supply to the PMT. Although it might be possible to reduce the total system fluctuation noise from ~1% to a half (~0.5%), it would be very difficult to reduce it down to a tenth

(~0.1%). This means that the ultimate precision in intensity measurements with the IP is of the order of 1%.

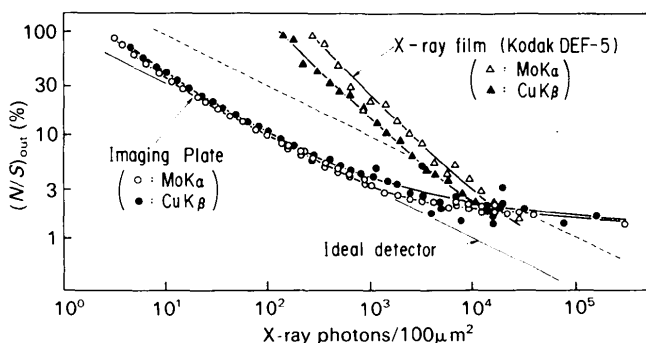


Figure 4 Relative uncertainty in the signal as a function of the exposure level. The circles correspond to the imaging plate and triangles to the X-ray film (Kodak DEF-5). The filled symbols are with 8.9 keV radiation and open symbols with 19.6 keV radiation. The solid line indicates a noiseless counter of 100% absorption efficiency (ideal detector). The dashed line indicates a noiseless counter of 10% absorption efficiency (Miyahara, Takahashi, Amemiya, Kamiya & Satow, 1988).

3.2. Dynamic range and linearity

Compared with X-ray film, the dynamic range of the IP is much wider, of the order of $1:10^5$ (Fig. 6). The response of the PSL is linear over the range from 8×10^1 to 4×10^4 photons/ $100 \mu\text{m}^2$, with an error rate of less than 5%. It should be noted that the dynamic range of the IP is extended towards the lower exposure levels of X-ray film, but not to the higher exposure levels. In practice, the dynamic range of the IP is limited to four orders of magnitude by that of the PMT during the readout. Two sets of PMTs are used to cover the entire dynamic range of the IP in the readout system, which is described in §4.

3.3. Spatial resolution and active-area size

The spatial resolution of the IP is $170 \mu\text{m}$ full width at half maximum (FWHM) of the line spread function (LSF). This value is obtained when the IP is read with a $100 \mu\text{m}$ laser-scanning pitch. The spatial resolution is determined mainly by laser-light scattering in the phosphor during the readout. The laser-light scattering originates from a mismatching of the refractive indices at the boundaries of phosphor crystal grains. For instance, even with a $50 \mu\text{m}$ scanning pitch of $50 \mu\text{m}$ laser-beam size, the spatial resolution is not improved in practice (about $150 \mu\text{m}$). For a higher spatial resolution, a different type of IP, a blue-colored IP, has been developed for use with electron microscopy. It includes blue pigments in the phosphor to minimize the scattering of laser light. With the blue-colored IP, a spatial resolution of slightly less than $100 \mu\text{m}$ is

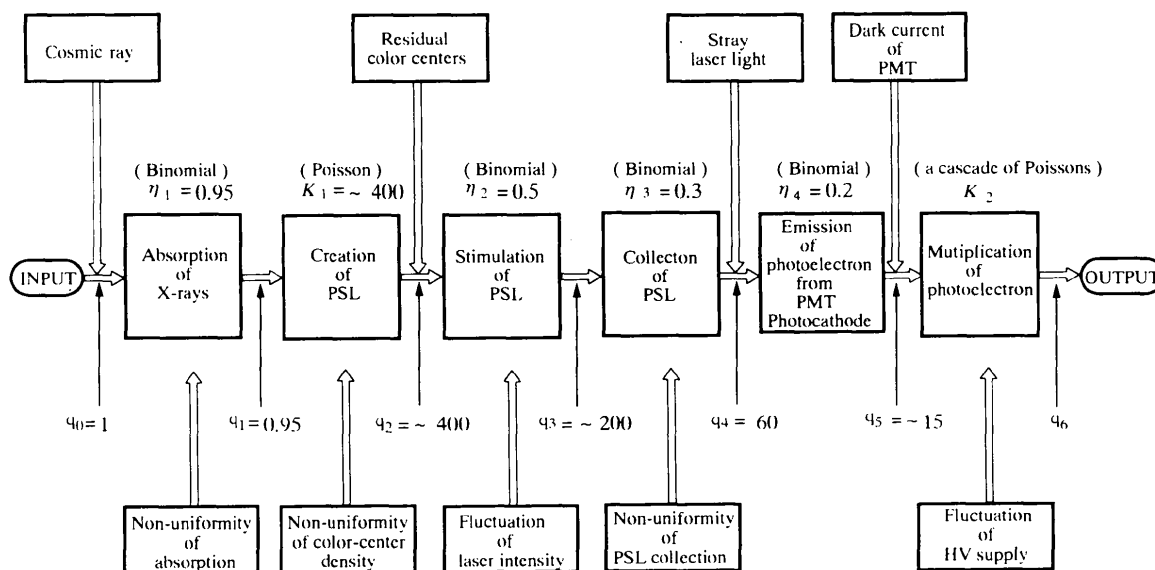


Figure 5 Diagram showing a cascade of stochastic elementary processes during X-ray exposure and image readout of the imaging plate. The probability distribution of each stochastic process is described in parentheses together with the mean value. The numbers of the quanta, q_i ($i = 0-5$) are also shown. The noise elements of the upper line contribute to the background noise which deteriorates the DQE at lower exposure levels. The noise elements of the bottom line contribute to the system fluctuation noise, which deteriorates the DQE at higher exposure levels.

realized, although the amount of PSL is decreased by about 30% compared with the standard IP. The tail of the LSF is spread like a Lorenzian shape, rather than a Gaussian shape. The extent of the tail depends largely on the type of laser scanner. With a typical flat-type laser scanner, the extent of the tail is about 1 mm at a 1% intensity level of the peak. It is as large as 4 mm at $\sim 0.1\%$ intensity level of the peak. The spread of the tail originates from the stimulation of highly concentrated color centers by stray light from the laser beam, which is intended to stimulate the nearby color centers. This effect is called 'flare', and careful attention should be paid when weak X-ray intensities around an intense X-ray beam have to be measured.

As to the active-area size of the IP, various standard sizes of the IP are commercially available, ranging from $127 \times 127 \text{ mm}^2$, $201 \times 252 \text{ mm}^2$, to $201 \times 400 \text{ mm}^2$. Recently, an IP readout system of size $800 \times 400 \text{ mm}^2$ has been developed for a Weissenberg camera at the Photon Factory by Sakabe *et al.* (1993).

3.4. Energy dependence

The amplitude of the IP signal per individual X-ray photon depends on the energy of the X-ray photons. It is considered to be proportional to the product of the absorption efficiency and the amount of energy deposited in the phosphor by an absorbed X-ray photon. The IP response per incident X-ray photon is shown as a function of the X-ray energy in Fig. 7. The unit of the ordinate is taken so that unity corresponds to the background noise level of the IP scanner, which is described in the next section. The deposited energy of an absorbed X-ray photon is obtained by dividing the IP response by the absorption efficiency of the phosphor. It is plotted as a function of the X-ray energy in curve (a) of Fig. 7. By observing curve (a), one can see that the energy deposited in the IP is abruptly decreased above the barium K absorption edge due to the energy lost through X-ray fluorescence. This effect is preferable

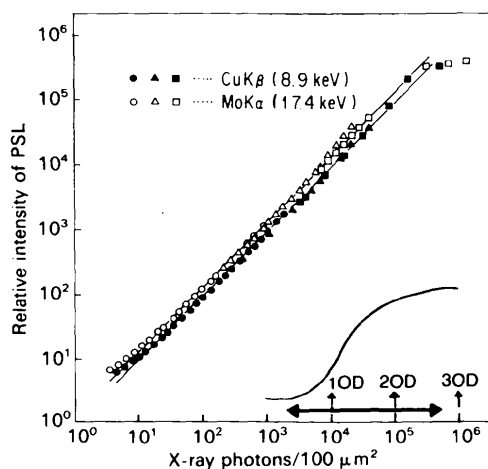


Figure 6 Dynamic range of the photo-stimulated luminescence of the imaging plate. The dynamic range of typical high-sensitivity X-ray film is also shown. OD refers to optical density.

because it will make the IP response curve smoother by compensating for the abrupt increase of the absorption efficiency at the edge. When different energies of X-rays are recorded in the IP, as in the case of Laue diffraction, the IP signals must be calibrated on the basis of curve (i) in Fig. 7 in order to obtain the X-ray intensity (the numbers of X-ray photons) of each X-ray energy.

3.5. Fading

Fading refers to the phenomenon in which the image stored in the IP decreases with time after exposure to X-rays. The fading rate depends on the temperature; it increases at higher temperatures. However, it does not depend on the exposure level or on the X-ray photon energy of the image. Fig. 8 shows the fading of an IP (type: BAS III) as a function of time for two different X-ray energies at 293 K. The fading curve is fitted with three exponentials:

$$I(t) = A_1 \exp(-k_1 t) + A_2 \exp(-k_2 t) + A_3 \exp(-k_3 t).$$

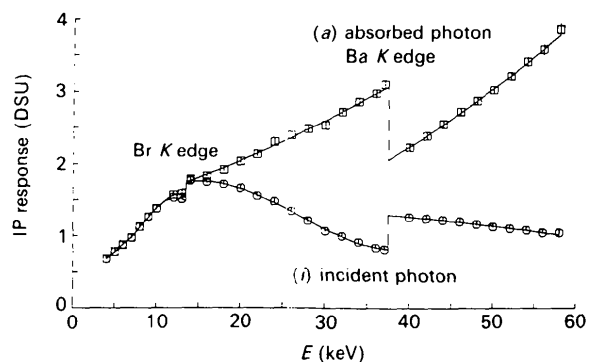


Figure 7 Dependence of the IP response as a function of the energy of an X-ray photon. (i) is the IP response per incident X-ray photon, and (a) the IP response per absorbed X-ray photon. The unit of the ordinate corresponds to the background noise level of the IP scanner (Ito & Amemiya, 1991).

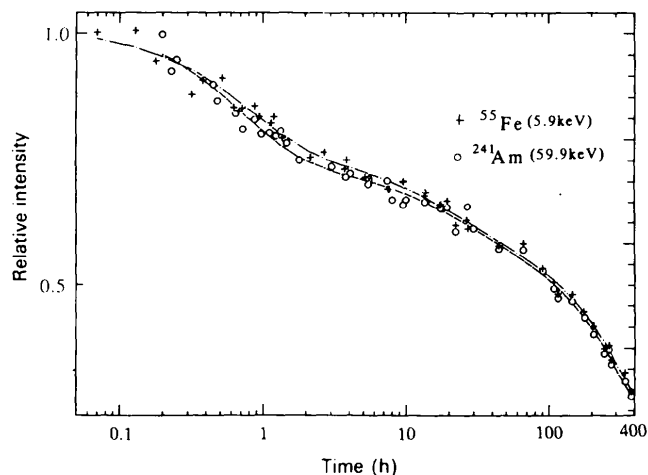


Figure 8 Fading of the IP signals as a function of time with two different X-ray energies (5.9 and 59.9 keV). Temperature: 293 K; type of IP: BAS III.

$1/k_1$, $1/k_2$ and $1/k_3$ are 0.7, 18 and 520 h, respectively. The characteristics of fading also depend on the type of IP, and results showing a faster fading rate were reported by Fujii *et al.* (1991). A detailed description of fading will appear elsewhere (Amemiya, Ogichi, Asano, Ito & Takahashi, 1994).

3.6. Other performance characteristics

The non-uniformity of the response of the IP is about 1–2% over an active area of $250 \times 200 \text{ mm}^2$. Unlike an X-ray TV camera and a gas-type area detector such as a multiwire proportional counter (MWPC), a correction for non-uniformity of response is not required. The distortion of the image depends on the type of IP scanner, and is usually of the order of 1%.

Since the IP is an integrating-type detector, it is free from the instantaneous count-rate limitations that accompany detectors operating in a pulse-counting mode. Therefore, the IP can make full use of the high flux of synchrotron X-ray radiation. However, irradiation of the IP with extremely intense X-rays (more than 10^{10} photons mm^{-2}) should be avoided. X-rays that are too intense create either non-erasable color centers, or color centers that are seemingly erasable but later reappear.

With minimum precautions, the IP yields reproducible results over long periods of repeated use, unlike X-ray film, whose performance is affected by slight changes in the development conditions. The mechanical flexibility of the IP is also very important when it is used with a Weissenberg camera.

4. Readout system

As is described in the previous section, the performance of the IP depends largely on that of the readout system. Various kinds of readout systems have been fabricated by several industrial companies, including the pioneering Fuji Photo Film Co. Ltd. The laser-scanning mode is categorized into three types: (i) a flat-type scanner in which the IP is kept flat while the laser beam scans the IP, (ii) an outer-drum-type scanner in which the IP is mounted on the outer

surface of a rotating drum, and (iii) an inner-drum-type scanner in which the IP is attached to the inner surface of a drum while the laser beam scans the IP. As an example, an outer-drum-type laser scanner which was developed at the Photon Factory is described here (Amemiya, Matsushita *et al.*, 1988) (Fig. 9).

A conventional drum-type film densitometer was modified. The IP, which stores an X-ray image, is attached to the outer surface of a drum of 400 mm circumference. A box which moves along the drum axis accommodates a 20 mW He–Ne laser source, a focusing optical system, two photomultiplier tubes (PMTs) and a device to collect the PSL. The output of the PMTs is logarithmically amplified and digitized by 100 kHz, 12-bit A/D converters. It takes 200 s to read the image on an IP of $250 \times 200 \text{ mm}^2$ with a pixel size of $100 \times 100 \mu\text{m}^2$. The parameters which are preset for reading an IP are, for a particular IP size, the sensitivity (the high voltage) of the PMTs, the pixel size and the rotation speed of the drum.

The system has the following characteristics: (a) The DQE is increased compared with a commercially available IP readout system using a total-reflecting glass assembly which efficiently collects the PSL. (b) Pixel sizes of $25 \times 25 \mu\text{m}^2$ and $50 \times 50 \mu\text{m}^2$ are available in addition to $100 \times 100 \mu\text{m}^2$ by making both the focus size and scanning pitch of the laser beam changeable. (c) A 12-bit A/D converter is used. The uncertainty in the intensity measurement due to the digitization process is as small as 0.22% when the system is preset to have the full range of the A/D converter correspond to four orders of magnitude. (d) In order to fully utilize a wide dynamic range of the PSL response, two PMTs with different sensitivities are used simultaneously to cover the entire intensity range of the PSL. (e) A flare around an intense spot is reduced by using the total-reflecting glass assembly. (f) Arbitrary sizes of IPs are available up to $400 \times 250 \text{ mm}$.

5. Time-resolved measurements using imaging plates

Inherently, the IP does not have a capability for the time-resolved recording of X-rays. However, when the IP is mechanically moved during an X-ray exposure, time-resolved measurements are possible. As examples, the two methods given below were developed: one is based on a cinema method which achieves a 0.3 s time resolution for 40 exposures of size $127 \times 127 \text{ mm}^2$; the other uses the IP as a linear detector which realizes a $23 \mu\text{s}$ time resolution for a time period of 46 ms, based on the streak-camera method.

5.1. Cinema method

The operating principles of the apparatus are similar to those of a movie camera. The apparatus consists of an IP exchanger, a fast X-ray shutter and a controller (Amemiya, Kishimoto, Matsushita, Satow & Ando, 1989).

Fig. 10 shows a schematic front view of the IP exchanger. IPs of $126 \times 126 \text{ mm}^2$ are exchanged one by one

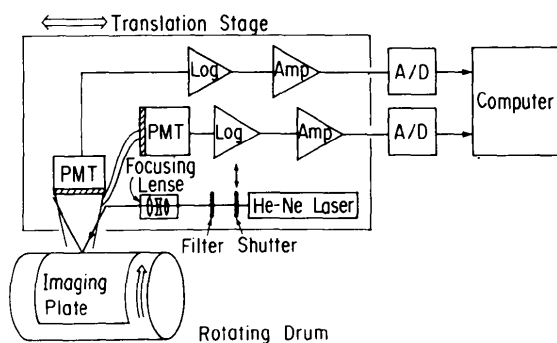


Figure 9
An outer-drum-type IP readout system.

at the position for X-ray exposure within a time of 0.2 s, during which a fast X-ray shutter, which is placed in front of the specimen, is closed. Unexposed IPs are individually mounted in plastic cassettes, and are stacked on edge in the right-hand bin. The foremost IP in the bin is pushed leftwards to the position for X-ray exposure (middle of the IP exchanger) by a motor-driven cam system. The IP at the position for X-ray exposure is again pushed leftwards into the left-hand bin by the next IP cassette, which is likewise pushed to the position for X-ray exposure. The minimum exposure time for each IP is 0.1 s and the dead-time between exposures is 0.2 s; thus, the system permits $3.3 \text{ exposures s}^{-1}$. A maximum of 40 IPs can be mounted in the bin.

The reproducibility of positioning the IP for X-ray exposure is within $\pm 50 \mu\text{m}$ in two orthogonal directions. This specification is important when the transient phenomenon of interest is repeatable, since it enables us to make multiple exposures on a set of IPs for better X-ray photon statistics.

This apparatus was applied to time-resolved small-angle X-ray scattering experiments from synthetic polymers under stretch (Amemiya, Satow *et al.*, 1988) and from contracting muscle under stretch and release. As an example, Fig. 11 shows four successive X-ray diffraction patterns from frog muscle during contraction under a slow stretch (Amemiya & Wakabayashi, 1991).

Another method for recording time-resolved two-dimensional patterns with IPs is a stroboscopic method in which a pulsed bunch of X-rays impinges upon the specimen at a particular time phase during a transient phenomenon of interest with the IP kept stationary. For this purpose, an ultra-fast X-ray shutter developed at CHESS (Legrand, Schildkamp & Blank, 1989) to isolate a single bunch of X-rays from synchrotron radiation is

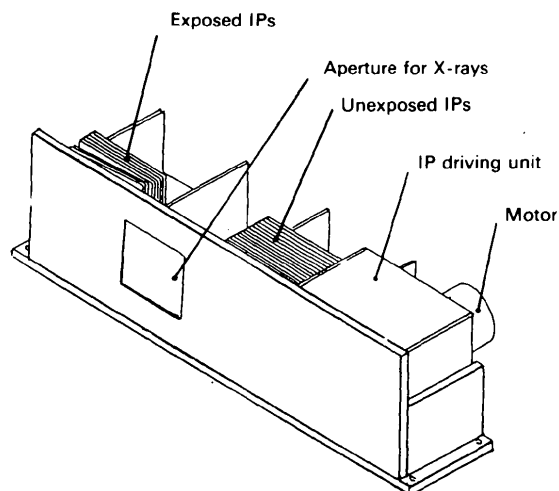


Figure 10
IP exchanger designed to record time-resolved two-dimensional X-ray patterns based on the cinema method; $3.3 \text{ exposures s}^{-1}$ are possible (Amemiya, Kishimoto, Matsushita, Satow & Ando, 1989).

very promising. With this method, a time resolution in the range of nanoseconds can be obtained for two-dimensional patterns.

5.2. Streak-camera method

This method is shown schematically in Fig. 12 (Amemiya, Kishimoto, Matsushita, Satow & Ando, 1989). An imaging plate is attached to a rotating drum with a circumference of 1080 mm. A one-dimensional X-ray diffraction pattern which passes through the receiving slit is recorded on the IP along the drum axis (the X axis), while intensity changes of the pattern as a function of time are recorded along the circumference (the T axis). Thus, time-resolved one-dimensional X-ray patterns are recorded as an X - T image on the IP. The size of the IP is 200 mm along the X axis and 1000 mm along the T axis. The time resolution and the number of time slices in the time-resolved measurement are determined by both the rotation speed of the drum and the vertical aperture of the receiving slit, as follows:

$$\text{Time resolution} = \text{rotation period} \times \text{slit aperture}/1080$$

and

$$\text{Number of time slices} = 1000/\text{slit aperture},$$

where the slit aperture is in mm. A time resolution of $23 \mu\text{s}$ per time slice is obtained for a duration of 46 ms when the drum rotates at its maximum speed of $20 \text{ rotations s}^{-1}$ with a 0.5 mm slit aperture.

There are four operational modes in the system: (i) exposure, (ii) read, (iii) erase and (iv) return. In the exposure mode, the drum rotates at a preset speed ranging from 20 to $0.01 \text{ rotations s}^{-1}$. The operation of the X-ray shutter and the timing of the trigger to the specimen is synchronized with the rotation of the drum. The aperture of the receiving slit is selected to fit with the vertical beam size.

After the exposure mode is finished, the X - T image recorded on the IP is read out with an He-Ne laser beam (10 mW), which scans the IP at a speed of about 10 m s^{-1} from behind the rotating drum.

In the erase mode, the IP with a residual image (about 50%) is irradiated with light from fluorescent lamps ($4 \times 15 \text{ W}$) while it is rotated on the drum. It takes about 10 min for the residual image to be completely erased. In the return mode, the position of the laser beam is returned along the X axis to the initial position for the next readout.

This apparatus was applied to time-resolved measurements of equatorial reflections from a contracting frog muscle (Fig. 13). Since the total intensity in the equatorial patterns exceeds $10^6 \text{ photons s}^{-1}$, experiments using gas-type linear detectors need to attenuate the incident X-rays. The time courses of the equatorial reflections of up to a (3,0) plane could be clearly observed with a time resolution of 1.4 ms and a repetition of only 50 cycles of muscle contraction. It was found that the times at which each of the intensity changes reaches its maximum are different from each other.

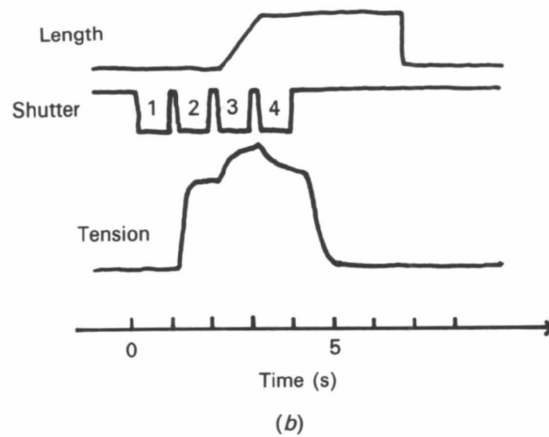
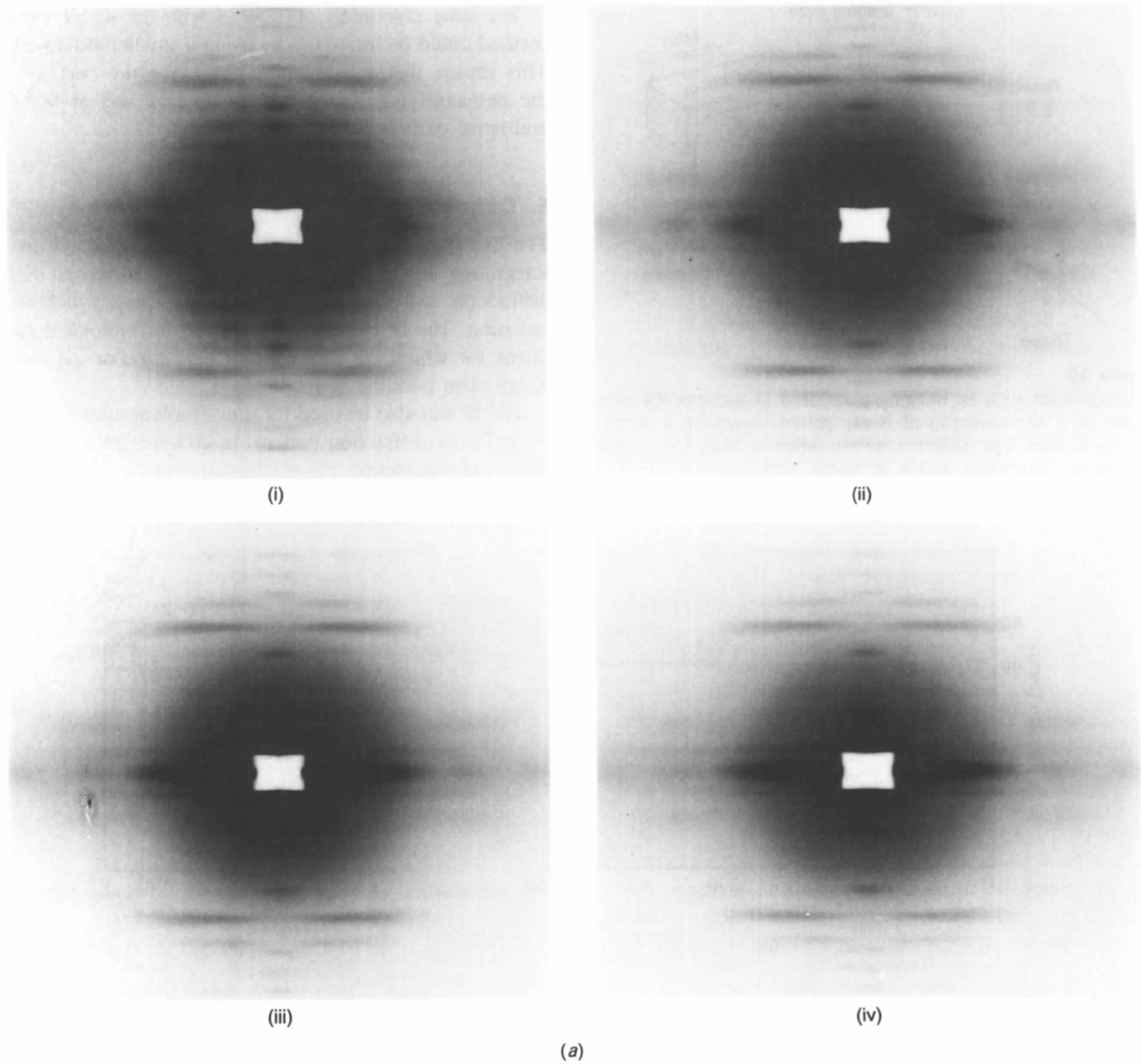
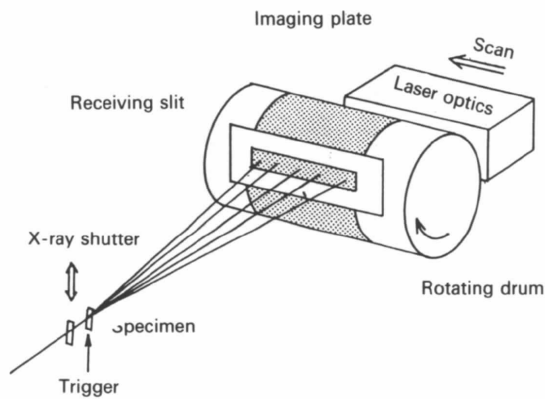


Figure 11

(a) Four successive X-ray patterns of frog muscle during contraction under stretch. (i) resting, (ii) contracting before stretch, (iii) contracting under stretch, and (iv) contracting after stretch. (b) Time chart of the experiment. From top to bottom: muscle length, shutter timing (exposure time = 0.8 s, interval between exposures = 0.2 s), and muscle tension. There were ten repetitions of contraction accumulated.

**Figure 12**

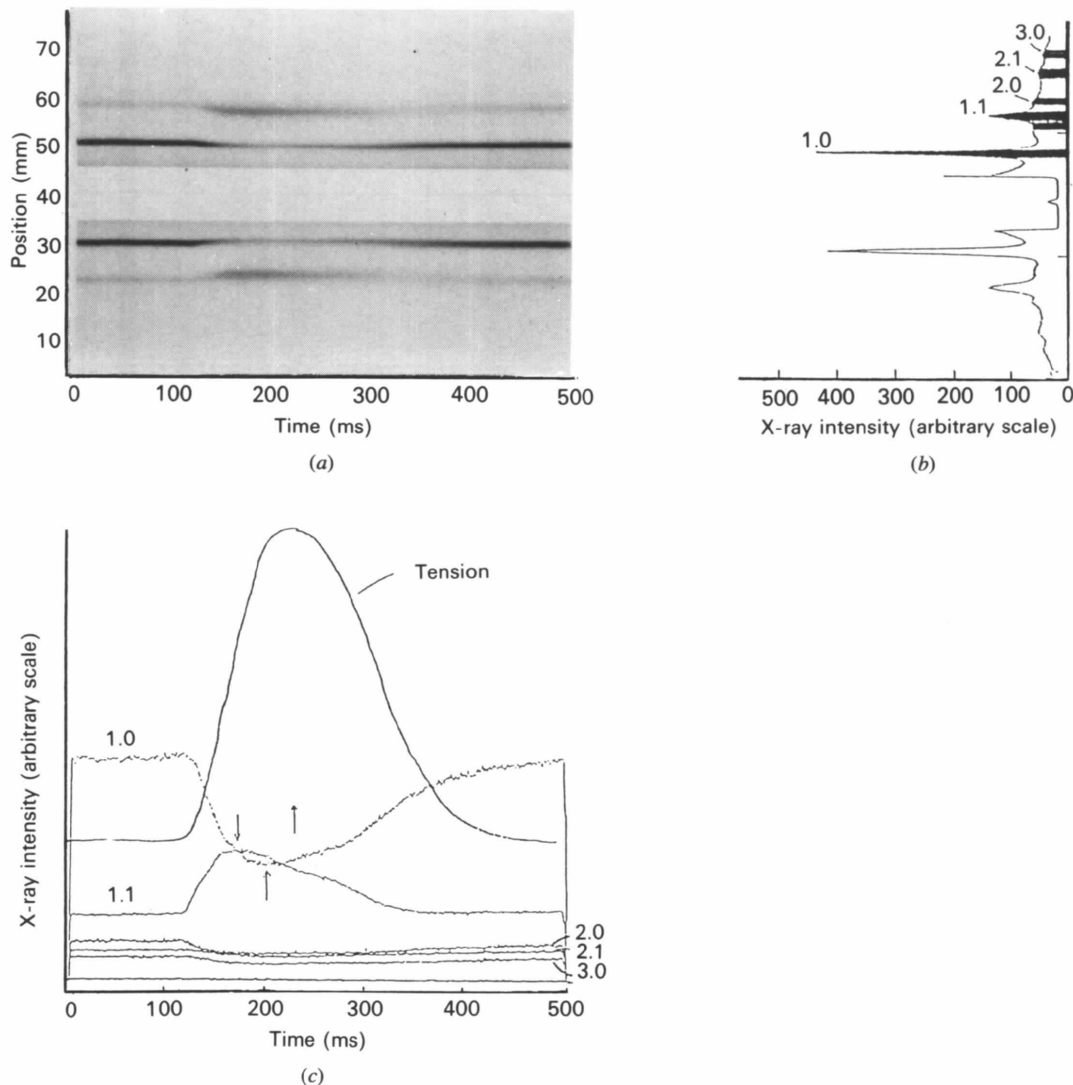
Rotating drum with an imaging plate used to measure the time course of a one-dimensional X-ray pattern based on a streak-camera method. The highest time resolution is $23 \mu\text{s}$ (Amemiya, Kishimoto, Matsushita, Satow & Ando, 1989).

The time resolution obtainable with the streak-camera method could be improved by using a smaller slit aperture. This means that this method can make the best use of the demagnifying X-ray optical systems and of the low emittance of 6–8 GeV storage rings.

6. Conclusions

The excellent performance characteristics of the IP as an integrating X-ray area detector are well suited to X-ray diffraction and scattering experiments using synchrotron radiation. The IP is particularly useful for biological specimens for which the shortest exposure time or the lowest X-ray dose possible is required.

The IP can also be used for time-resolved measurements of an X-ray diffraction pattern, to complement its uses in static measurements.

**Figure 13**

Time-resolved X-ray pattern of equatorial reflections from a frog muscle during a twitch contraction: time resolution = 1.39 ms , number of contractions = 50. (a) X-T image, (b) intensity profile along the X axis, (c) time courses of reflection intensities. The arrows indicate the times when the intensity changes are maximum (Amemiya, Kishimoto, Matsushita, Satow & Ando, 1989).

A combination of two powerful tools, synchrotron radiation and imaging plates, has mutually enhanced their potentials. The IP has replaced standard X-ray film and some other X-ray detectors, which were conventionally used in synchrotron radiation applications. Examples include X-ray diffraction under high pressure and high temperature (Shimomura *et al.*, 1987), Compton scattering (Itoh *et al.*, 1989), dispersive EXAFS and X-ray diffuse scattering. X-ray topography and X-ray microscopy will also benefit from the IP when the spatial resolution is improved to a few tens of micrometers in FWHM.

When more intense X-rays are available from insertion devices installed in 6–8 GeV storage rings, the IP system will continue to play a more important role as one of the best X-ray area detectors because of its high DQE and lack of any instantaneous count-rate limitations.

References

- Amemiya, Y., Kishimoto, S., Matsushita, T., Satow, Y. & Ando, M. (1989) *Rev. Sci. Instrum.* **60**, 1552–1556.
- Amemiya, Y., Matsushita, T., Nakagawa, A., Satow, Y., Miyahara, J. & Chikawa, J. (1988). *Nucl. Instrum. Methods*, **A266**, 645–653.
- Amemiya, Y. & Miyahara, J. (1988). *Nature (London)*, **336**, 89–90.
- Amemiya, Y., Ogichi, T., Asano, Y., Ito, M. & Takahashi, K. (1994). In preparation.
- Amemiya, Y., Satow, Y., Matsushita, T., Chikawa, J., Wakabayashi, K. & Miyahara, J. (1988). *Synchrotron Radiation in Chemistry and Biology*, Vol. II, edited by E. Mandelkow, pp. 121–144. Berlin: Springer-Verlag.
- Amemiya, Y. & Wakabayashi, K. (1991). *Adv. Biophys.* **27**, 115–128.
- Amemiya, Y., Wakabayashi, K., Tanaka, H., Ueno, Y. & Miyahara, J. (1987). *Science*, **237**, 164–168.
- Fujii, I., Morimoto, Y., Higuchi, Y., Yasuoka, N., Katayama, C. & Miki, K. (1991). *Acta Cryst.* **B47**, 137–144.
- Ito, M. & Amemiya, Y. (1991). *Nucl. Instrum. Methods*, **A310**, 369–372.
- Itoh, F., Sakurai, M., Sugawa, T., Suzuki, K., Sakai, N., Ito, M., Mao, O., Shiotani, N., Tanaka, Y., Sakurai, Y., Nanao, S., Kawata, H., Amemiya, Y. & Ando, M. (1989). *Rev. Sci. Instrum.* **60**, 2402–2405.
- Legrand, A. D., Schildkamp, W. & Blank, B. (1989). *Nucl. Instrum. Methods*, **A275**, 442–446.
- Miyahara, J. (1989). *Chem. Today*, (10), 29–36. (In Japanese.)
- Miyahara, J., Takahashi, K., Amemiya, Y., Kamiya, K. & Satow, Y. (1986). *Nucl. Instrum. Methods*, **A246**, 572–578.
- Sakabe, N. (1987). *Acta Cryst.* **A43**, C-8.
- Sakabe, N., Sakabe, K., Higashi, T., Nakagawa, A., Watanabe, N. & Adachi, S. (1993). *Acta Cryst.* **A49**, C-12.
- Shimomura, O., Takemura, K., Fujimura, T., Hase, K., Kikegawa, T., Ohishi, Y., Okuyama, K., Shiba, S., Fujii, Y., Matsushita T. & Amemiya, Y. (1987). *Photon Fact. Act. Rep.* **5**, 161.
- Sonoda, M., Takano, M., Miyahara, J. & Kato, H. (1983). *Radiology*, **148**, 833–838.